UNIVERSITY *of* York

This is a repository copy of *Polar oxide/semiconductor heterojunction:MgO (111)/SiC (0001)*.

White Rose Research Online URL for this paper:
https://eprints.whiterose.ac.uk/id/eprint/231522/

Version: Published Version

Article:

White Rose
university consortium
Universities of Leeds, Sheffield & York

eprints@whiterose.ac.uk
https://eprints.whiterose.ac.uk/

Polar oxide/semiconductor heterojunction: MgO (111)/SiC (0001)

Julio A. do Nascimento ; Daniel Pingstone; Adam Kerrigan ; Kenta Yoshida; Aleksandar Skeparovski ; Katherine S. Ziemer; Yihong Chen; Kelvin H. L. Zhang ; Martin Stankovski; Demie Kepaptsoglou; Philip Hasnip ; Zlatko Nedelkoski ; Vlado K. Lazarov ✉

Check for updates

View Online

Export Citation

AIP Publishing

Polar oxide/semiconductor heterojunction: MgO (111)/SiC (0001)

View Online　　Export Citation　　CrossMark

Julio A. do Nascimento,[1] (iD) Daniel Pingstone,[1] Adam Kerrigan,[1] (iD) Kenta Yoshida,[2] Aleksandar Skeparovski,[3] (iD)
Katherine S. Ziemer,[4] Yihong Chen,[5] Kelvin H. L. Zhang,[5,6] (iD) Martin Stankovski,[1] Demie Kepaptsoglou,[7]
Philip Hasnip,[1] (iD) Zlatko Nedelkoski,[8] (iD) and Vlado K. Lazarov[1,3,a)] (iD)

AFFILIATIONS

[1]School of Physics, Engineering, and Technology, University of York, Heslington, YO10 5DD, York, United Kingdom

[2]Institute for Materials Research, Tohoku University, Ibaraki 311-1313, Japan

[3]Institute of Physics, Faculty of Natural Sciences and Mathematics, Ss. Cyril and Methodius University, Arhimedova 3, Skopje, North Macedonia

[4]Chemical Engineering Department, Northeastern University, Boston, Massachusetts 02115, USA

[5]State Key Laboratory of Physical Chemistry of Solid Surfaces, College of Chemistry and Chemical Engineering, Xiamen University, Xiamen 361005, China

[6]Department of Chemistry, Inorganic Chemistry Laboratory, University of Oxford, South Parks Road, Oxford OX1 3QR, United Kingdom

[7]SuperSTEM, Sci-Tech Daresbury Campus, Daresbury WA4 4AD, United Kingdom

[8]Faculty of Technical Sciences, Mother Theresa University, 1669 11A Skopje, North Macedonia

[a)]Author to whom correspondence should be addressed: vlado.lazarov@york.ac.uk

ABSTRACT

The layered structures of polar oxides (i.e., metal/oxygen/metal/oxygen/…) can be utilized to engineer the atomic structures and thus tailor the electronic properties of polar oxide/semiconductor interfaces, including the band offsets between the technologically important MgO and SiC for complementary metal–oxide–semiconductor and spintronic devices. However, the growth of atomically flat polar oxide MgO films with arbitrary thickness has been hindered by polarity issues. In this study, we analyze the interfacial structure and band alignment of MgO (111) thin films deposited on 6h-SiC (0001) by the molecular beam epitaxy method. An epitaxial growth of the MgO (111) thin film on SiC is demonstrated. We show that the interface is O-terminated by atomic-scale scanning transmission electron microscopy measurements. The insulating characteristics are preserved in the vicinity of the interface according to electronic structure calculations. X-ray photoelectron spectroscopy measurements show that the valence band offset is approximately 1.6 eV. Electronic structure calculations for a realistic model constructed using the atomically resolved electron microscopy images show an excellent agreement between the calculated and measured valence band offsets, further confirming the validity of the developed atomic interface model. These findings pave the way for further advancements in MgO-based electronic devices, considering the ability to tailor the interface atomic structure, which could be employed to engineer the overall electronic properties at the interface, including the valence band offset.

Wide-bandgap semiconductors such as SiC and GaN are of significance for device applications that require high-temperature operations, high frequency, and high power density.[1–4] One of the main challenges for their use in power transistor applications is the lack of a suitable oxide for metal–oxide–semiconductor types of structures. Particularly, the native oxide (SiO_2) of SiC has a smaller dielectric constant than SiC, which limits the operation to considerably below the

breakdown voltage of SiC.[5] In addition, the electronic properties of the SiO_2/SiC interface are rather poor due to the high density of surface/interface trap states, which significantly decreases the carrier mobility in SiC gate channels.[6] Therefore, the provision of an oxide with a high dielectric constant and chemical and thermal stabilities and low interface density of states is crucial for both SiC and GaN device technologies. Several oxides, such as MgO and Al_2O_3, have garnered attention

12 September 2025 12:50:10

due to their excellent thermal properties and high dielectric constants.[7,8]

MgO has been proposed as an oxide barrier for SiC-based devices due to its high dielectric constant $k \sim 10$, low lattice mismatch with SiC of only 3%, and spin filtering properties.[9–16] The low lattice mismatch between MgO and SiC minimizes interfacial strain, which is conducive to reduced leakage currents in high-power devices. Moreover, the polar MgO (111) can form atomically abrupt and almost defect free interfaces with GaN (0001), GaN (111), and SiC (0001).[17] The layered structure of the polar oxide (i.e., metal/oxygen/metal/oxygen/…) can be utilized to engineer the atomic interface structure, and thus tailor the electronic properties of the polar oxide/semiconductor interface including the band offsets between MgO and SiC or GaN.

Intrinsically polar materials, such as metal oxides and compound semiconductors, are used in numerous electronic, magnetic, and chemical applications. However, along the polar direction, they consist of oppositely charged ionic planes, which leads to diverging electric dipole moments with the increase in film thickness, according to electrostatic models.[18] Various mechanisms that overcome the polarity issue have been reported, including surface reconstruction, surface faceting, surface metallization, and adatoms.[18–21] In numerous studies on MgO growth along its polar [111] orientation, as well as in other rock salt oxides,[21] surface roughening has been observed, including faceting into neutral surface planes, as a mechanism to overcome the polarity.[22–25] The presence of adatoms such as H could efficiently quench the surface dipole moment of some polar oxide surfaces, including MgO (111), leaving them in a (111) termination.[26–28] In this regard, H has been employed as a surfactant, providing a dynamical solution for the polarity constraints throughout the growth of MgO (111).[29] This H surfactant approach can enable the growth of single-crystal MgO (111) films and pave the way for the growth of polar oxide heterostructural devices with improved electronic properties. Furthermore, the hexagonal symmetry of MgO (111) films in combination with the good thermal stability, relatively high dielectric constant, and spin filtering properties could provide complementary metal–oxide–semiconductor and spintronic devices based on wide-bandgap semiconductors and ferrite oxides.

In this study, we demonstrate an epitaxial growth of an MgO (111) thin film on a SiC substrate, with a unique atomic stacking at the interface. Atomic-scale scanning transmission electron microscopy (STEM) measurements show the O termination of the interface, while x-ray photoelectron spectroscopy (XPS) measurements show that the valence band offset (VBO) is $\sim$1.6 eV. Electronic structure calculations, performed on a realistic model based on atomic-scale STEM images, show an excellent agreement between the calculated and measured VBOs, which further validates our atomic interface model. In addition, the electronic calculations show the absence of interface states.

The MBE growth was performed on n-type 6h-SiC wafers. The SiC substrate was annealed in hydrogen gas under high-vacuum conditions to obtain an atomically flat SiC(0001) surface. For the annealing, the SiC substrate was heated to 900 °C under a molecular hydrogen pressure of 5×10^{-8} mbar. The base pressure of the system was 2×10^{-10} mbar. The gas pressure was measured using an ion gauge and residual gas analyzer. The samples were heated by direct-current resistive heating. The substrate temperature during deposition

was $\leq$200 °C. H was used to passivate the dangling bonds on the SiC surface. This approach removes scratches and extends surface terraces of the SiC, i.e., extends SiC surface step edges due to the saturation of dangling bonds at step edges.[24] In addition, the hydrogen adsorbed on the substrate surface can act as a surfactant for the layer-by-layer MgO growth.[29]

MgO thin films were grown using the plasma-assisted molecular beam epitaxy method. The deposition consisted of a simultaneous exposure of the substrate to magnesium and oxygen. Magnesium was deposited from a Createc low-temperature effusion cell, set to 280 °C, at a rate of $\sim$2 Å/min, determined using a calibrated quartz crystal microbalance. Oxygen was provided in a plasma form from an Oxford Applied HD-25 plasma source operated at 90 W. The oxygen pressure in the system was 1×10^{-6} mbar, measured by an ion gauge. To avoid silica nucleation, the substrate was first exposed to magnesium flux followed by the oxygen plasma at a pressure of 10^{-6} mbar.

XP spectra were acquired using a monochromated Al K$_\alpha$ x-ray source with an electron beam flood gun to minimize surface charging and enable a reliable charge offset correction. The spectra were charge-corrected using a gold reference and carbon 1s reference from SiC. The valence band maxima for the SiC and MgO were measured using a bulk SiC reference and a 20 nm thick MgO film grown on SiC, respectively. The SiC substrate signal is completely suppressed as the inelastic mean free path of photoelectrons is significantly smaller than the film thickness. The core energy levels for Mg 2p and Si 2p were measured using the bulk references and compared to the core level values measured for the MgO/SiC thin film interface to calculate the VBO. The s-orbitals were measured as bonding states for the VBO calculations by Eq. (1). The s-states were measured to improve the energy resolution, as the signals from the $2p$ states of Si and Mg are small. XPS core level data were fitted using a split pseudo-Voigt function, which is a modified Gaussian function that accounts for asymmetry in the data peak due to the removal of the Shirley background. Further information on the growth and XPS data analysis is provided in the supplementary material (supplementary material Notes S1 and S2, Figs. S4–S6).

Atomic-resolution imaging was performed using the Nion UltraSTEM100 aberration-corrected dedicated scanning transmission electron microscope, operated at 100 kV with a convergence angle of 30 mrad. At these optical conditions, the electron probe size is determined to be 0.9 Å. The inner detector angle for high-angle annular dark field (HAADF) STEM imaging was 76 mrad. HAADF images were acquired by a rigid registration as stacks of images of the same area recorded in quick succession, resulting in a high signal-to-noise ratio and precision in the image. Additional bright-field (BF) TEM imaging was performed with a double-aberration-corrected JEOL JEM-2200FS operating at 200 kV. The samples were prepared by conventional cross section polishing methods followed by further thinning using ion milling to achieve electron transparency. HAADF image simulations were performed by the QSTEM multislice code[30] to compare model structures to observations, using the experimental optical and specimen conditions as input parameters.

Electronic structure simulations were performed with the CASTEP code[31] to compare VBOs to the measured values. To compensate for the electric dipole moment in the modeled MgO structures, hydroxyl terminations were used as a terminating layer. To analyze the positions of the bands at the interface, the valence band edges were

computed separately for bulk SiC and MgO cells with respect to their averaged potentials and offset for the calculated potential difference across the interface of the supercell model. The G_0W_0 calculations were performed on the bulk SiC and MgO by the abinit code[32] to take into account many-body effects in the determination of the VB energy edge.

Figure 1 shows BF TEM images of the grown MgO/SiC. The BF low-magnification image, in Fig. 1(a), shows an overall cross-sectional view of the sample, which demonstrates the constant thickness of the film and abrupt interface between the MgO film and SiC substrate. The higher-magnification high-resolution (HR) TEM image in Fig. 1(b) shows the single-crystal structures of the film and substrate and further confirms the abruptness of the interface without the formation of secondary amorphous oxide phases, including SiO_x. These TEM images confirm the feasibility of our approach for the growth of epitaxial MgO(111) thin films on SiC, with an epitaxial relation of MgO(111)||SiC(0001) and MgO(1-10)||SiC(11-20) (Fig. S1), and demonstrate that the employed method overcomes the polarity issues.

Considering the strong dependence of the electronic properties on the interfacial atomic structure, we acquired a HAADF STEM image of the MgO film on the SiC substrate, presented in Fig. 2, to determine the interfacial termination structure.

The HAADF STEM imaging technique, due to its $\sim Z^2$ atomic column intensity dependence on the atomic number Z, provides direct identification of atomic columns. The presented image outlines the atomically abrupt interface, with a clear distinction between the film and substrate, Fig. 2(a). The analysis of the film's atomic columns shows the difference between the intensities of Mg and O. The STEM image [Figs. 2(a) and 2(b)] shows a row of atomic columns with a reduced intensity at the interface, matching that of an oxygen plane in the MgO film, as confirmed by an image simulation [Fig. 2(c)] performed using the QSTEM simulation package on a model with an O top-site interface [overlaid in Fig. 2(b)]. The intensity profile in Fig. 2(e) for the region in Fig. 2(d) selected from Fig. 2(a) better reflects the O termination of the MgO film.

We also carried out a first-principle analysis of the formation energies of different possible O atomic site populations at the interface
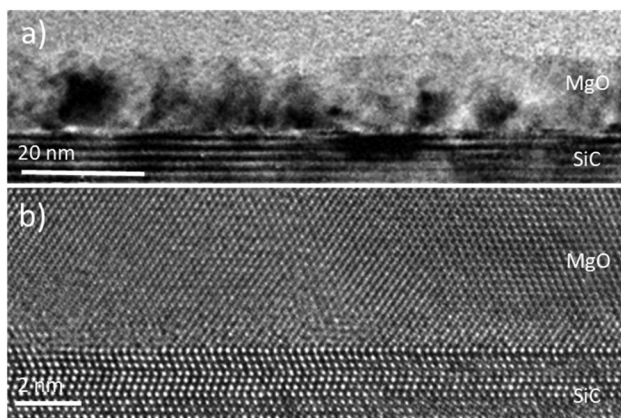
FIG. 1. (a) Low-magnification bright-field TEM image of the MgO film grown on SiC and (b) higher-magnification HRTEM image of the MgO(111)/SiC(0001) heterostructure.

[T4, H3, and top site; supplementary material Fig. S2 and Fig. 2(b)]. The T4 configuration has 3.0 eV/supercell higher formation energy than the top-site configuration, while the formation energy difference between the H3 configuration and top-site configuration is 1.9 eV/supercell. These results further confirm that the top-site O configuration is more stable than the T4 and H3 configurations, as expected according to the measured STEM image. The distance between the first interfacial Mg and Si planes is larger by $\sim 15\%$ than the distance between neighboring Mg planes in the interior part of the MgO film, while the corresponding value obtained by the simulation for the developed top-site model is $\sim 14\%$, which further shows the validity of our model.

The partial local densities of states (PDOSs) in Fig. 3 projected by atomic species show the absence of detrimental interface states near the Fermi level. In other words, the insulating characteristics of both film and substrate are preserved at the interface region. Similar behaviors are obtained for the O-terminated interfaces with interfacial O atoms at T4 and H3 sites, as shown in supplementary material Fig. S2.

Figure 4 shows XP spectra of three sets of specimens, a bare SiC(0001) and thin (2.5 nm) and thick (20 nm) MgO(111) films/SiC(0001), acquired to determine the valence and conduction band offsets. TEM images of the thin (~ 2.5 nm) and thick (~ 20 nm) MgO(111) films/SiC(0001) are presented in Fig. S3. The dashed lines represent fittings employed to accurately determine the energy values of core levels and valence band maxima. The valence band maximum is determined by the energy value at the intercept where the linear fit crosses the baseline signal. Figure 4(a) shows the 2s core level results for both Si and Mg measured from the thin MgO film. The binding energies measured using these peaks are in agreement with those in the NIST XPS database[33] for SiC and MgO. Figure 4(b) shows the measurement results for the "bulk" 20 nm thick MgO film. The binding energy measured for the fitted peak corresponds to the Mg 2s energy state in MgO. The valence band maximum was determined by interpolation as the spectrum approaches the valence band edge. Figure 4(c) shows results as in (b) but for the SiC Si 2s and valence band maximum reference.

Based on these results, in Fig. 5, we illustrate the band alignment at the interface of MgO and SiC with the band offsets, ΔE_c and ΔE_v. The bandgap energies of 6h-SiC and MgO are also presented. For MgO/SiC, the calculation of the VBO was carried out by the following equation:

$$E_{VBO} = \left(E_{2s}^{Si} - E_{2s}^{Mg}\right)_{HJ} - \left(E_{2s}^{Si} - E_{VBM}^{Si}\right)_{SiC} + \left(E_{2s}^{Mg} - E_{VBM}^{Mg}\right)_{MgO},$$

(1)

where HJ denotes the heterojunction, while the values for the parameters are obtained using the XPS results. The VBO obtained by the measured energy positions of Mg 2s and Si 2s and the respective valence band maxima is 1.62 eV. This value reasonably well agrees with that reported by Goodrich (1.50 eV),[34] which indicates that the VBO measurements based on the s and p orbitals are comparable.

Furthermore, calculations were performed with the CASTEP code to predict the VBO for the model constructed according to the measured STEM image. Oxygen is in the top-site position on the SiC surface, where the next C atom would be positioned if the 6h structure of SiC is continued. The calculated VBO is 1.60 eV [Fig. 5(b)], in excellent agreement with the measured VBO, which further confirms the
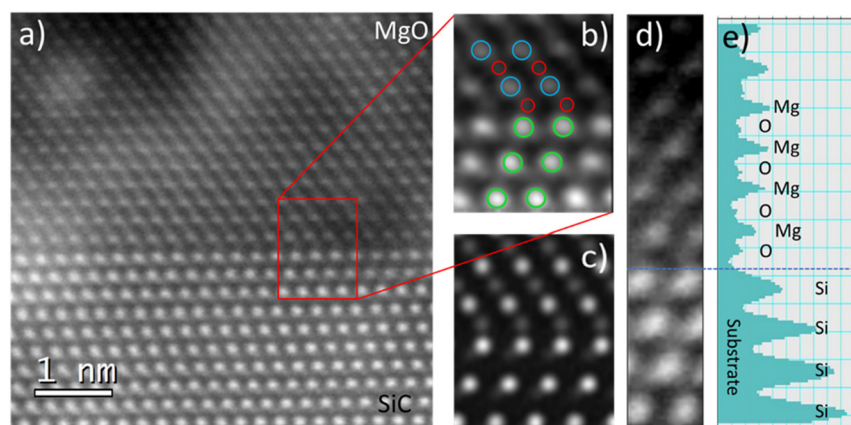
FIG. 2. (a) HAADF STEM image at the interface, (b) its magnified view with an overlaid structural model with the oxygen top-site interface termination (Si: green, O: red, and Mg: blue), (c) corresponding HAADF STEM image simulated using QSTEM, and (d) and (e) region selected from (a) and corresponding average intensity profile along the vertical direction showing the O termination of the MgO film, respectively.
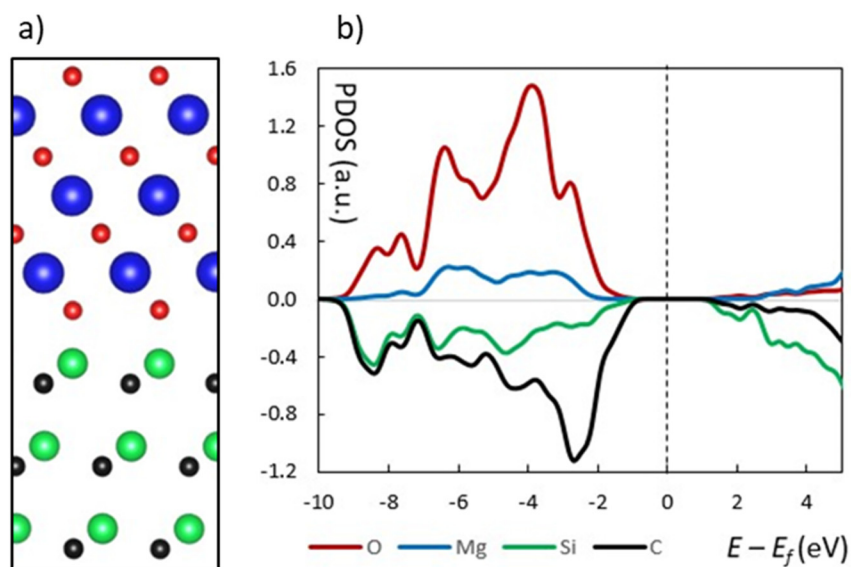
FIG. 3. (a) Structural model for the O top-site interface (Si: green, C: black, O: red, and Mg: blue) and (b) PDOSs for the different atomic species at the interface. The Fermi level is indicated by the dashed black line.
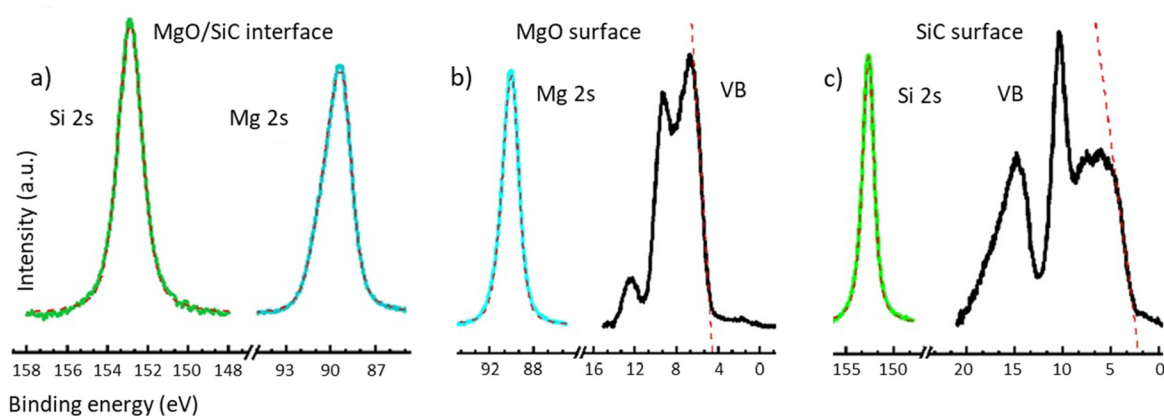
FIG. 4. (a) XP spectrum acquired from the MgO/SiC thin film interface. Using this spectrum, the core level difference in Eq. (1) is calculated with the binding energies of the Mg 2s and Si 2s orbitals. (b) XP spectrum acquired from a 20 nm thick MgO film on SiC, used as a bulk reference for the Mg core levels and valence band maximum. (c) XP spectrum acquired from SiC to determine the same properties as in (b).

FIG. 5. (a) Schematic of the band alignment for the MgO/SiC interface, constructed using the XPS results. VB: valence band, CB: conduction band, and HJ: heterojunction. (b) In-plane-averaged potential as a function of the distance from the interface plane. The valence band positions are indicated by the thick red lines.

validity of the developed atomistic model for the investigated MgO/SiC heterostructure. In contrast to the measured and calculated values of the VBO in this study, Zhang *et al.* have reported a VBO of 3.65 eV for SiC-4h/MgO.[35] This VBO difference could be assigned to the different interfacial atomic structures of the heterostructures in this study and their study. Therefore, the experimental and theoretical results obtained in this study suggest that the VBO is significantly modified by the presence of oxygen at the interface. These findings indicate that the electronic structures, including the band offset, could be engineered by carefully tailoring the interfacial atomic structure.

In this study, we demonstrated an epitaxial growth of a MgO (111) thin film on a SiC substrate. Atomic-scale STEM measurements revealed that the interface is O-terminated. The insulating characteristics are preserved in the vicinity of the interface according to the electronic structure calculations. According to the XPS measurements, the VBO is approximately 1.6 eV. Electronic structure calculations using the model based on the measured STEM image showed an excellent agreement between the calculated and measured VBOs, which further confirms the validity of our model. These findings pave the way for further advancements in MgO-based electronic devices, considering the ability to tailor the interface atomic structure, which could be employed to engineer the overall electronic properties at the interface, including the VBO.

See the supplementary material for details on the diffraction pattern of the MgO/SiC heterostructure, atomic structures and PDOSs for T4 and H3 interface models, TEM images of the ~2.5 and ~20 nm thick MgO films, detailed growth procedure, effects of hydrogen treatment, TEM images of a film obtained by a nonoptimized growth procedure, and characterization of a thicker specimen.

AUTHOR DECLARATIONS
Conflict of Interest

The authors have no conflicts to disclose.

Author Contributions

Julio A. do Nascimento: Data curation (equal); Formal analysis (equal); Writing – original draft (equal); Writing – review & editing (equal). **Daniel Pingstone:** Data curation (equal); Formal analysis (equal); Writing – original draft (equal). **Adam Kerrigan:** Formal analysis (equal). **Kenta Yoshida:** Data curation (equal). **Aleksandar Skeparovski:** Formal analysis (equal). **Katherine S. Ziemer:** Data curation (equal). **Yihong Chen:** Data curation (equal). **Kelvin H. L. Zhang:** Data curation (equal). **Martin Stankovski:** Formal analysis (equal). **Demie Kepaptsoglou:** Data curation (equal); Resources (equal). **Philip Hasnip:** Formal analysis (equal); Resources (equal). **Zlatko Nedelkoski:** Formal analysis (equal); Writing – original draft (equal); Writing – review & editing (equal). **Vlado K. Lazarov:** Conceptualization (equal); Formal analysis (equal); Funding acquisition (equal); Resources (equal); Writing – original draft (equal); Writing – review & editing (equal).

DATA AVAILABILITY

The data that support the findings of this study are available from the corresponding author upon reasonable request.

REFERENCES

[1] F. Roccaforte, P. Fiorenza, G. Greco, R. L. Nigro, F. Giannazzo, A. Patti, and M. Saggio, Phys. Status Solidi A **211**(9), 2063–2071 (2014).

[2] M. Bhatnagar and B. J. Baliga, IEEE Trans. Electron Devices **40**(3), 645 (1993).

[3] H. Matsunami, Microelectr. Eng. **83**(1), 2–4 (2006).

[4] S. Yuvaraja, V. Khandelwal, X. Tang, and X. Li, Chip **2**(4), 100072 (2023).

[5] G. D. Wilk, R. M. Wallace, and J. M. Anthony, J. Appl. Phys. **89**, 5243–5275 (2001).

[6] Y. Yeo, T. King, and C. Hu, IEEE Trans. Electron Devices **50**(4), 1027–1035 (2003).

[7] O. N. Ogidi-Ekoko, J. C. Goodrich, A. J. Howzen, M. R. Peart, N. C. Strandwitz, J. J. Wierer, Jr., and N. Tansu, Solid-State Electron. **172**, 107881 (2020).

[8] A. Calzolaro, T. Mikolajick, and A. Wachowiak, Materials **15**(3), 791 (2022).

[9] C. Su, M. Frederick, M. Menghini, L. Dillemans, R. Lieten, T. Smets, J. W. Seo, and J. Locquet, Thin Solid Films **520**(14), 4508–4511 (2012).

[10] P. J. van Der Zaag, P. J. H. Bloemen, J. M. Gaines, R. M. Wolf, P. A. A. van Der Heijden, R. J. M. van de Veerdonk, and W. J. M. De Jonge, J. Magn. Magn. Mater. **211**(1–3), 301–308 (2000).

[11] S. Ikeda, J. Hayakawa, Y. Ashizawa, Y. M. Lee, K. Miura, H. Hasegawa, M. Tsunoda, F. Matsukura, and H. Ohno, Appl. Phys. Lett. **93**(8), 082508 (2008).

[12] Y. M. Lee, J. Hayakawa, S. Ikeda, F. Matsukura, and H. Ohno, Appl. Phys. Lett. **90**(21), 212507 (2007).

[13] R. Jansen, J. Phys. D **36**(19), R289 (2003).

[14] A. Tsukazaki, A. Ohtomo, T. Kita, Y. Ohno, H. Ohno, and M. Kawasaki, Science **315**(5817), 1388–1391 (2007).

[15] A. A. Baker, A. I. Figueroa, D. Pingstone, V. K. Lazarov, G. Van Der Laan, and T. Hesjedal, Sci. Rep **6**, 35582 (2016).

[16] S. Yuasa, T. Nagahama, A. Fukushima, Y. Suzuki, and K. Ando, Nat. Mater. **3**(12), 868 (2004).

[17] V. K. Lazarov, J. Zimmerman, S. H. Cheung, L. Li, M. Weinert, and M. Gajdardziska-Josifovska, Phys. Rev. Lett **94**, 216101 (2005).

[18] C. Noguera, J. Phys. **12**, R367 (2000).

[19] J. Goniakowski, F. Finochi, and C. Noguera, Rep. Prog. Phys. **71**, 016501 (2008).

[20] V. E. Henrich and P. A. Cox, *The Surface Science of Metal Oxides* (Cambridge University Press, Cambridge, 1994).

[21] A. Kerrigan, K. Pande, D. Pingstone, S. A. Cavill, M. Gajdardziska-Josifovska, K. P. McKenna, M. Weinert, and V. K. Lazarov, Appl. Surf. Sci. **596**, 153490 (2022).

[22] O. Maksimov, P. Fisher, M. Skowronski, P. A. Salvador, M. Snyder, J. Xu, and X. Weng, J. Cryst. Growth **310**, 2760–2766 (2008).

[23] M. Kiguchi, S. Entani, K. Saiki, T. Goto, and A. Koma, Phys. Rev. B **68**, 115402 (2003).

[24] T. L. Goodrich, J. Parisi, Z. Cai, and K. S. Ziemer, Appl. Phys. Lett. **90**, 042910 (2007).

[25] K. Matsuzuki, H. Hosono, and T. Susaki, Phys. Rev. B **82**, 033408 (2010).

[26] V. K. Lazarov, R. Plass, H.-C. Poon, D. K. Saldin, M. Weinert, S. A. Chambers, and M. Gajdardziska-Josifovska, Phys. Rev. B **71**, 115434 (2005).

[27] H. C. Poon, X. F. Hu, S. E. Chamberlin, D. K. Saldin, and C. J. Hirschmugl, Surf. Sci. **600**, 2505 (2006).

[28] K. Refson, R. A. Wogelius, D. G. Fraser, M. C. Payne, M. H. Lee, and V. Milman, Phys. Rev. B **52**, 10823 (1995).

[29] V. K. Lazarov, Z. Cai, K. Yoshida, K. H. L. Zhang, M. Weinert, K. S. Ziemer, and P. J. Hasnip, Phys. Rev. Lett. **107**, 056101 (2011).

[30] C. T. Koch, Ph.D. thesis, Arizona State University, 2002.

[31] S. J. Clark, M. D. Segall, C. J. Pickard, P. J. Hasnip, M. I. J. Probert, K. Refson, and M. C. Payne, Z. Kristallogr. Cryst. Mater. **220**(5/6), 567–570 (2005).

[32] X. Gonze *et al.*, Comput. Phys. Commun. **248**, 107042 (2020).

[33] See https://srdata.nist.gov/xps/main_search_menu.aspx for "NIST X-ray Photoelectron Spectroscopy Database, Version 3.5."

[34] T. L. Goodrich, "Atomistic investigation into the interface engineering and heteroepitaxy of functional oxides on hexagonal silicon carbide through the use of a magnesium oxide template layer for the development of a multifunctional heterostructure," Ph.D. thesis (Northeastern University Boston, Massachusetts, 2008).

[35] B. L. Zhang, F. F. Cai, G. S. Sun, H. B. Fan, P. F. Zhang, H. Y. Wei, X. L. Liu, S. Y. Yang, Q. S. Zhu, and Z. G. Wang, Appl. Phys. Lett. **93**, 072110 (2008).

12 September 2025 12:50:10